

# Evaluation of bending limit curves of aluminium alloy AA6014-T4 and dual phase steel DP600 at ambient temperature

Krishna Kumar Saxena<sup>1</sup> · Ipsita Madhumita Das<sup>1</sup> · Jyoti Mukhopadhyay<sup>1</sup>

Received: 11 June 2015 / Accepted: 5 October 2015 / Published online: 22 October 2015  
© Springer-Verlag France 2015

**Abstract** Bending/hemming operations are extensively used in automotive industries for assembling the car body panels. Besides the process mechanics, bending operation differs from biaxial sheet metal forming operations in failure mechanism also. Hence, the limit strains that material can sustain are different for both the operations. Thus, the conventional FLC proposed by Keeler and Goodwin fails to predict formability in bending/hemming operations. This necessitates the development of bending limit curves. In this work, bending limit curves are determined experimentally for AA6014-T4 and DP600. Effect of punch radius, nature and level of pre-strain on the bending limits is also studied. Thus, BLC can be used as a post-processing criterion in finite element simulations to assess formability during bending/hemming operations.

**Keywords** Formability · FLC · Bending limit curve

## Introduction

The increasing demand for light weight vehicles has increased the use of Al 5000 & 6000 series and dual phase

steels in outer and inner body panels of automobiles. The automotive panels are manufactured using sheet metal forming operations. Bending and hemming operations are used to join adjacent car body panels. After the forming of the car body panels, it is necessary to focus on the edges (Fig. 1) which are subjected to bending/hemming operations. The dominant load on these edges during hemming or bending is plane strain.

Besides process mechanics, bending and hemming operations differ from biaxial forming in failure mechanism also. In biaxial forming, failure takes place due to membrane instability, which involves necking (Fig. 2a). On the other hand, failure in bending and hemming operations involves inter-crystalline fracture (Fig. 2b). Thus, the conventional forming limit curve, as proposed by Keeler [1] & Backofen [2] and Goodwin [3] fails to predict the formability in bending or hemming operations.

The Forming limit curve is a graphical tool applied to sheet metal forming processes to determine the limit strains which can be imposed on a sheet metal before plastic instability occurs. The FLC depicts the combination of major and minor strains showing safe/failure region when sheet metal is stretched over rigid punch. Denninger [4], Schleich [5] and Liewald [6] have mentioned in their work that the FLC fails to assess formability in bending or hemming operations due to difference in failure mechanisms. FLC investigation is based on simple membrane shell theory which doesn't take into account the effect of sheet bending.

Furthermore, it has been shown experimentally that bending limits are higher than forming limits [5]. Hence, it is necessary to develop a bending limit curve to assess formability in bending operations. BLC is determined by applying stretching and bending loads simultaneously on the material. The BLC can be used as a post-processing criterion in finite element based simulations in the same manner as FLC. The region

---

✉ Krishna Kumar Saxena  
krishnasxn@gmail.com

Ipsita Madhumita Das  
ipsita.das@iitgn.ac.in

Jyoti Mukhopadhyay  
jm@iitgn.ac.in

<sup>1</sup> Department of Materials Science and Engineering, Indian Institute of Technology Gandhinagar, Ahmedabad, India



**Fig. 1** The edges of automobile panel (*red colour*) which are subjected to bending/hemming operations

below the BLC results in safe bending whereas region above BLC represents a failed geometry during bending or hemming. Figure 3 shows representation of combined BLC and FLC. It can be easily visualized that bending limits are higher than forming limits.

Sarkar et al. [7, 8] calculated the tensile properties and bendability of AA6111 and AA5754 alloys. They found that, the alloys with lower Fe content show good bendability, whereas alloys with higher Fe content show low bendability in case of pre-strained condition. Concept of bending limit curve was first introduced by Liewald et al. [9]. Lin et al. [10] predicted bendability and hemmability from plain strain tensile test. Kitting et al. [11] characterized stretch bending deformation with respect to tool radius and stretching condition by performing angular stretch bend Test (ASBT). However, effect of tool radius on bending deformation couldn't be identified properly, as different uniaxial stretching conditions prevail in varying the tool radius. In modified ASBT, stretching conditions were found to be independent of tool radius. Maout et al. [12] performed various numerical simulations in multistep hemming processes. This was followed by Hu et al. [13], who developed a 3D numerical model to simulate bending by laser peen forming. Later critical volume fraction criterion was found to be an important parameter to predict bending cracks [14]. Pedersen et al. [15] studied the fracture mechanism of AA7075-T651 alloy under different loading conditions. They observed the

quasi-static dynamic fracture behavior of AA7075 alloy and found that it depends on grain morphology, orientation of rolling direction and intermetallic coarser particles. Zadpoor et al. [16] observed the bending of monolithic sheets and tailor made blanks along with effect of sheet thickness on their forming limit. Failure strain was observed to decrease with increase in sheet thickness. However, they concluded that pre-straining doesn't have a significant effect on bendability of specimen. Furthermore, shearing facilitated across the particle stringers can be a cause of decreased bendability in case of continuously casted 5754 aluminium alloy and decreased strength was accounted due to particle stringers. Also, the bending angle decreases with increase in specimen thickness. Davidkov et al. [17] experimented on strain localization and damage development of AA5754 alloy sheet and suggested that the maximum plastic strain below the free surface of the specimen can be accounted for interaction between propagation of shear in the matrix and second phase particle stringers. Denninger [18] evaluated the bendability of a material in terms of bending limit curve and studied the change in BLC level due to different pre-strain paths. Bending models such as flow theory model and deformation theory model were studied by He et al. [19] and they concluded that flow theory is more consistent with stretch bending operation. Shi et al. [20] analyzed the failure of fusion clad alloy system AA3003/AA6XXX sheet under bending and determined the effect of particle distribution on bending behavior with transverse bending axis. Liewald and Drotleff [21] presented the fundamental behavior of BLC along with the three dimensional failure surface for combined BLC. In the present work, bending limit curves are experimentally determined for AA6014 and DP600 with punch radius of 0.4 and 2 mm. The regression model is developed to evaluate the bending limit in arbitrary bending ratios. The effect of punch radius as well as nature and level of pre-strain is studied.

### Forming limit curves of Al6014 and DP600

The forming limit curves of Al6014-T4 and DP600 are shown in Fig. 4. These FLCs were obtained by Nakazima test as per

**Fig. 2** Magnified images of cracks showing failure due to **a** membrane instability **b** inter-crystalline fracture (Schleich et al.2009)

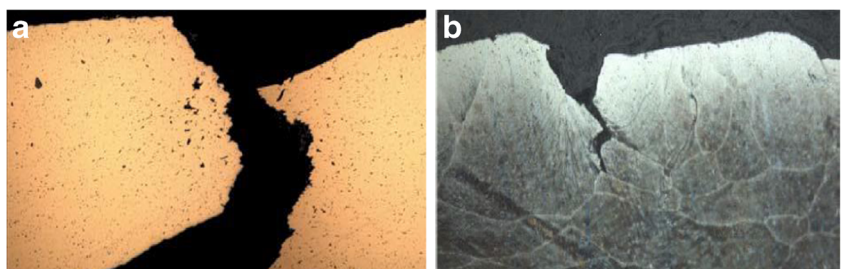
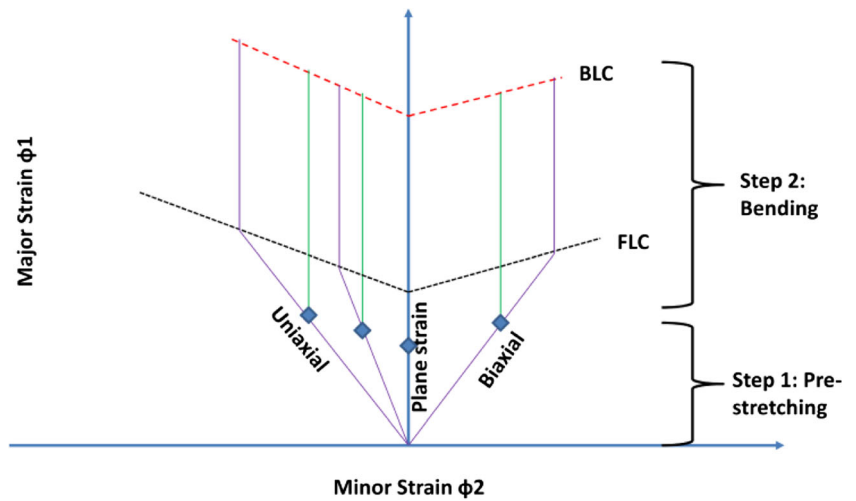


**Fig. 3** Representation of combined BLC and FLC



ISO12004-2 standard [22]. It can be observed from the FLCs that both Al6014-T4 and DP600 possess a good combination of stretchability-drawability.

Furthermore, it can be seen from both the experimental and simulated sample (Figs. 5 and 6) that the failure was due to membrane instability or necking. It can be observed in Fig. 6 that the severe thinning (yellow colour) leads to rise of cracks and finally failure takes place (red colour).

The failure zones in Fig. 5 were magnified using optical microscopy. The evidences of ductile shear failure due to necking & thinning can be seen in Fig. 7a and b. It can be observed from Fig. 7a that thinning has occurred on the edges of failure zone whereas evidences of ductile shear failure can be observed on the cross-section as in Fig. 7b. Thus, FLC is not suitable for evaluating formability in bending/hemming operations as bending failure is due to trans-crystalline fracture.

**Experimentation**

For present investigation, Al6014 and DP600 alloy with an initial sheet thickness of 1.04 mm were used. These alloys are extensively used in the outer and inner body panels respectively of cars. Al 6014 is a typical Al-Mg-Si alloy and is characterized by an excellent formability and bendability. The composition of Al 6014 alloy is shown in Table 1.

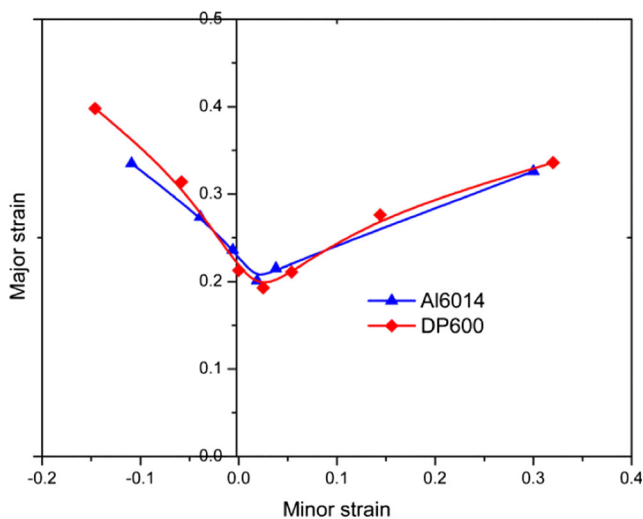


**Fig. 4** FLC for Al6014 and DP600



**Fig. 5** Failure zone in experimental sample

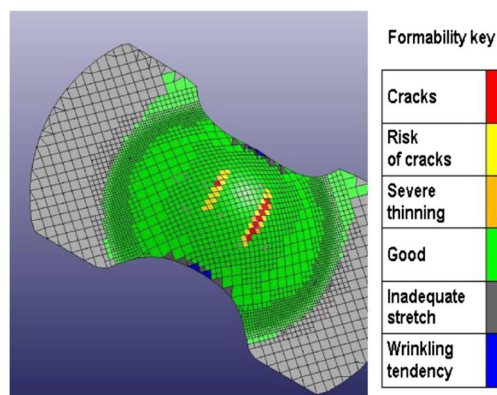


**Fig. 6** Failure zone in simulated sample. (LS Dyna)

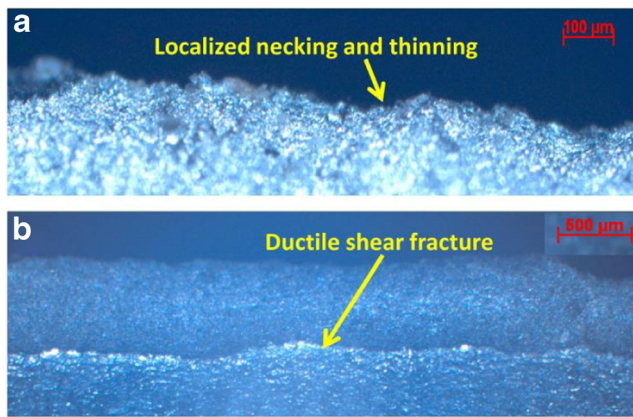


**Fig. 7** Magnified images of failure zones in Nakazima sample given in Fig. 6, showing evidences of ductile failure due to membrane instability **a** localized necking and thinning as observed from failure surface (100x) **b** ductile shear fracture as observed from cross-section (25x)

DP600 is a low carbon steel, alloyed with a relatively high level of manganese plus some Si and Cr to promote the formation of DP microstructure (martensite-ferrite). DP600 is an important automotive material due to its unique mechanical properties such as continuous yielding behaviour, a lower ratio of yield/tensile strength, superior combination of strength and ductility, good formability and a higher initial work hardening rate as compared to other HSLA steels with similar chemical composition. Table 2 shows the composition of DP600 alloy.

Uniaxial tensile tests were conducted as per ASTM E8 [23] standard. The specimens were cut in  $0^\circ$ ,  $45^\circ$  &  $90^\circ$  orientation to rolling direction. Figure 8 shows the specimen used for uniaxial tensile test.

For the above experimentation cross head velocity was kept as 48 mm/min. Strains in the specimen were measured using DIC technique. The specimens were spray painted with black & white speckle pattern. Tables 3 and 4 depict the uniaxial properties for Al6014 and DP600 respectively as determined from uniaxial tensile tests.

It can be observed from uniaxial data that Al6014 possess high value of strain hardening exponent which signifies that Al6014 has more ability to distribute strain uniformly. On the other hand DP600 has low  $n$  value which signifies that it has less capability to distribute strain uniformly as compared to Al6014. Aluminium has highest strength parallel to rolling direction whereas DP600 has highest strength transverse to rolling direction. The yield ratio (YS/UTS) of both the materials is fairly good.

**Table 1** Composition (wt %) of Al 6014

Element	Si	Fe	Cu	Mn	Mg	Cr	Zn	Ti
wt (%)	0.3–0.6	0.35 max	0.25 max	0.05–0.2	0.4–0.8	0.2 max	0.1 max	0.05 max

**Table 2** Composition (wt %) of DP600

Element	C	Mn	Si	Cr	Ni	P	S
wt (%)	0.12	1.8	0.44	0.26	0.016	0.021	0.006

The microstructures of Al6014-T4 and DP600 as obtained using standard metallographic procedure are shown in Figs. 9 and 10 respectively. Al6014-T4 (0.8 % Mg) is a highly diluted aluminium alloy. The magnesium to silicon ratio is properly balanced (1.8:1) to form magnesium silicide ( $Mg_2Si$ ). [24]. In case of dual phase steel, dual microstructure can be seen. The ferritic grains are surrounded by martensitic islands.

To analyze the bending operation, whole strain path of the forming process: from pre-stretching to bending of the material was taken into account. In order to obtain a BLC, a three point bend test according to VDA 238–100 [25] was carried out. For reliable results, the critical scenario for bending operation was chosen i.e., the specimen was bent transverse to rolling direction. First, the specimens were pre-stretched on the Marciniak press in the uniaxial, plain strain and biaxial directions. From the pre-strained samples, square specimens of dimensions 50 \* 50 mm were cut out as shown in Fig. 11. The strain gradient on the pre-strained flat specimens was evaluated using DIC technique from GOM Aramis software. Five sections were superimposed and equivalent Von-Mises strain was plotted along these sections. Figure 12 shows the variation of equivalent pre-strain with section length for a sample pre-strained to 5 % strain. Similarly this was carried out for all the specimens to ensure that the material was reached the desired level of pre-straining.

The level of pre-stretching used for Al6014 and DP600 is shown in Table 5. The authors were able to carry out the bend tests after 6 days of pre-straining tests. The specimens were kept in material storage room for 6 days at room temperature. Thus in this short duration, the aging kinetics is unlikely to affect the strength.

Bend tests were performed by installing a three point bend test setup on the IFU uniaxial tensile testing machine (Fig. 13a). The experiments were performed with two bending punches of radii 0.4 and 2 mm respectively. Before the test, specimens were painted with speckle pattern. The specimen was mounted on two rollers in such a way that it was aligned in centre and parallel to bending punch as shown in Fig. 13b.



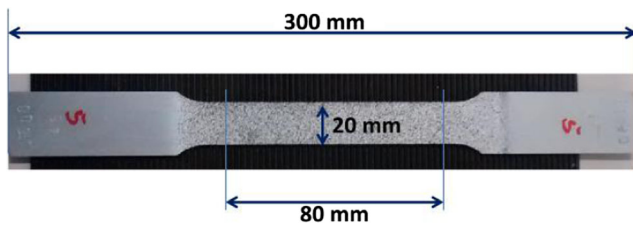


**Fig. 8** Uniaxial tensile test specimen

Test was stopped, the moment punch force drops to 50 N. The bending limits were determined using DIC technique with the help of GOM Aramis software. Three sections were superimposed on the bent edge after the bending operation as shown in Fig. 14. The bending strain was plotted along these sections.

The maximum strain reached along the section was taken as the bending strain for BLC. Three samples for each pre-straining level were tested for accuracy. The specimens after three point bend tests are shown in Fig. 15. Equivalent pre-strain for the specimens was calculated using Eq. 1 [26].

$$\phi_{eq} = \sqrt{\phi_1^2 + \phi_2^2 + \phi_1\phi_2} \tag{1}$$

Bending limit strains for both of the materials were determined using punch radii of 0.4 and 2 mm. These bending limit strains were plotted to get the respective BLCs in major strain and minor strain space. The total bending strain or bending limit strain is calculated as the sum of the pre strain and the maximum strain after bending as in Eq. 2.

$$\phi_{BL} = \phi_{1p} + \phi_b \tag{2}$$

To ensure reliability, pure experimental results have been reported to plot BLCs without incorporating any correction factor. For the sake of simplicity, the complete experimental approach to evaluate BLC is shown in Fig. 16.

## Results and discussion

### Bending limit curve for Al6014

Figure 17 shows the bending limit curves for Al6014 for punch radii of 0.4 and 2 mm. To get complete picture of

**Table 3** Tensile properties of Al6014

Orientation with respect to rolling direction	n (Strain hardening exponent)	Yield strength (MPa)	Ultimate tensile strength (MPa)	Yield ratio
0°	0.249	130.35	233.90	0.557
45°	0.250	128.50	230.82	0.557
90°	0.253	126.61	229.20	0.552

**Table 4** Tensile properties of DP600

Orientation with respect to rolling direction	n (Strain hardening exponent)	Yield strength (MPa)	Ultimate tensile Strength (MPa)	Yield ratio
0°	0.171	382.76	668.31	0.573
45°	0.177	394.65	677.60	0.582
90°	0.172	395.16	683.08	0.579

formability, combined bending and forming limit curves are plotted. It can be observed that the bending limits are much higher than the forming limits due to difference in failure mechanisms and process mechanics. This confirms that FLCs fail to evaluate bendability. Furthermore, it can be seen from Fig. 17 that the level of BLC is higher for lower punch radius. This is because punch with lower radius imposes higher strains on the outer fibre (Fig. 18) during bending which results in brittle fracture. It is in conformation to the observations made by Denninger et al. [18]. As shown in Fig. 18, high strains of tensile nature are generated on the outer fiber of the bent specimen during bending. However, the inner most fiber suffers from compressive strain.

Figure 19 shows the plot between total bending strain and equivalent pre-strain. Initially, it is observed that with increase of pre-strain, bending strain decreases. This can be explained on the basis of the fact that the secondary particles present in the Al6014 alloy are sheared away during pre-straining. It is found that with further increase in pre-strain level, bending strain again increases. This increase in bendability is due to the dominant reduction of sheet thickness at a constant inner radius. The rate of increase in bending strain with respect to pre-strain also varies due to evolution of damage during bending.

It is clear from Figs. 17 and 19 that total bending strain is a function of nature & level of pre-strain as well as punch radius. Variation of total bending strain with respect to equivalent pre-strain and strain ratio ( $\alpha$ ) is shown in Figs. 20 and 21. From the contour plots, it can be

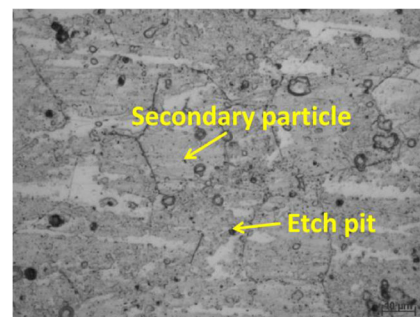


**Fig. 9** Microstructure of Al6014

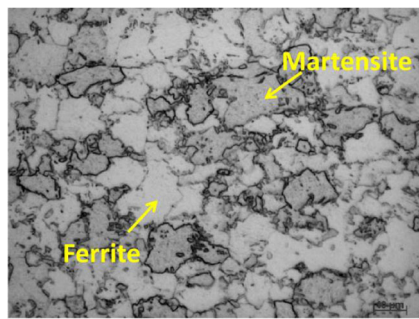


Fig. 10 Microstructure of DP600

observed that at higher level and uniaxial nature of pre-straining, total bending strain is maximum in case of Al6014 for both 0.4 and 2 mm bending radii. Lower bending strains are observed at lower level and biaxial nature of pre-straining. Strain ratio ( $\alpha$ ) is defined as the ratio of minor strain ( $\phi_2$ ) to major strain ( $\phi_1$ ) and is represented in Eq. 3.

$$\alpha = \frac{\phi_2}{\phi_1} \tag{3}$$

**Bending limit curve for DP600**

Figure 22 represents the bending limit curve for DP600 combined with FLC. It can be observed that bending limits for DP600 also are much higher than the forming limits. Furthermore, higher bending strains are achieved with uniaxial pre-straining as compared to biaxial pre-straining. BLC level is higher for lower punch radius as it imposes higher strain on the outer fibre of the specimen. BLC is constructed by keeping account of all nature of loading. It can be observed from Fig. 22 that on plane strain axis, the two limit strains for 0.4 and 2 mm are outlier from the

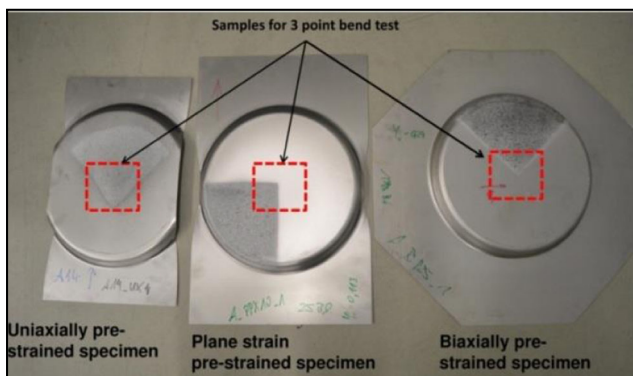


Fig. 11 Cutting of specimens for bend test from the pre-strained Marciniak specimens

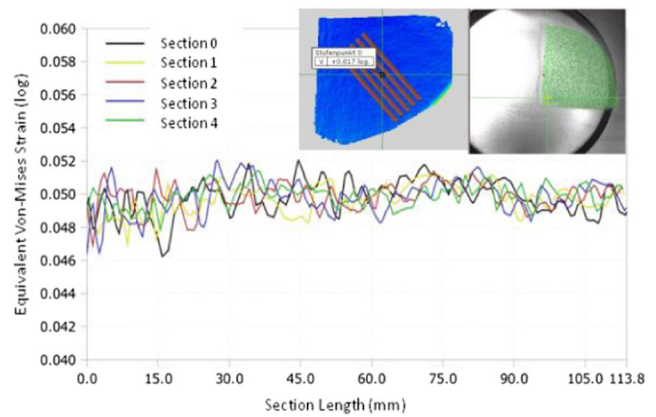


Fig. 12 Strain gradient along the section length for biaxial pre-straining of 5 %

BLCs. This is due to the two successive plane strain loadings of the samples. DP600 has the higher flexural strength, so the bending limit strains for plane strain loading are very high. In real forming process, plane strain loading is rare. So this doesn't question the reliability of the curve.

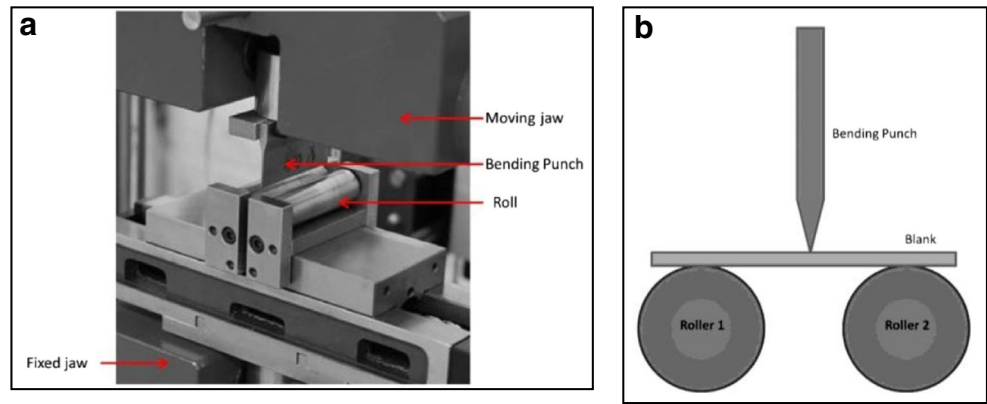
Figure 23 shows the plot between total bending strain and equivalent pre-strain. The increasing trend of bending strain with respect to equivalent pre-strain can be observed in this plot. This is due to the superior strain hardening capability of dual phase steels. Due to the dual microstructure, formability of dual phase steels is higher. The increase in bendability of DP600 with increasing pre-strain can be attributed to the reduction in sheet thickness at a particular bend radius. Hence, strains are higher near the bent edge.

Total bending strain of DP600 depends on punch radius, flexural strength and pre-strain level. Variation of total bending strain & strain ratio is shown in Figs. 24 and 25 with the help of contour plots. For 0.4 mm bending radii, at higher level and uniaxial nature of pre-straining, higher bending strains are observed. On the other hand, for 2 mm bending radii; at lower level of pre-straining and plane strain condition, higher bending strains are observed. However, lower bending strains are observed at extreme uniaxial and biaxial nature and lower level of pre-straining for 0.4 mm bending radii. For 2 mm bending radii

Table 5 Level of pre-straining for bend test

Type of pre-straining	UPX (Uniaxial) (%)	PPX (Plain strain) (%)	BPX (Biaxial) (%)
Al6014	5, 10, 15	10	2, 5, 15, 25
DP600	5, 9, 20	5	5, 15, 20

**Fig. 13** Three-point bend test used for experimentation. **a** Bend test setup (Courtesy: IFU). **b** Schematic diagram of bending device



lower bending strains are observed at lower level and bi-axial nature of pre-straining only.

**Regression model for total bending strain**

It is important to make the BLC applicable to arbitrary loading ratios. For this purpose, regression model was used. Total bending strain is the sum of major pre-strain and bending strain component. Total bending strain, given by Eq. 2.

Equivalent pre-strain and strain ratio are presented in Eq. 1 and 3 respectively. Total bending strain can be given as a function of equivalent pre-strain ( $\phi_{eq}$ ), strain ratio ( $\alpha$ ) and punch radius ( $r$ ) as shown in Eq. 4.

$$\phi_{BL} = f(\phi_{eq}, \alpha, r) \tag{4}$$

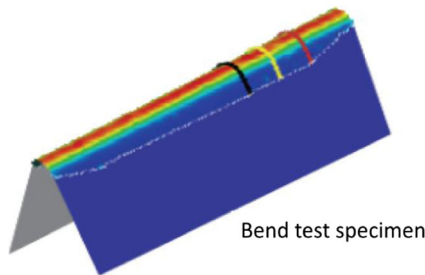


**Fig. 14** Measurement of bending strain from GOM Aramis by superimposing the section on the bent edge of the specimen. (Courtesy: IFU)

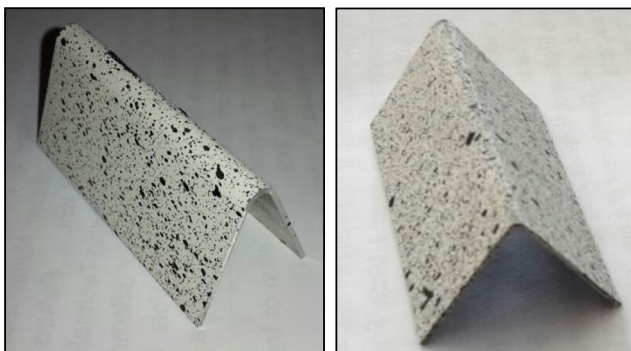


**Fig. 15** Bend test specimens after three point bend test

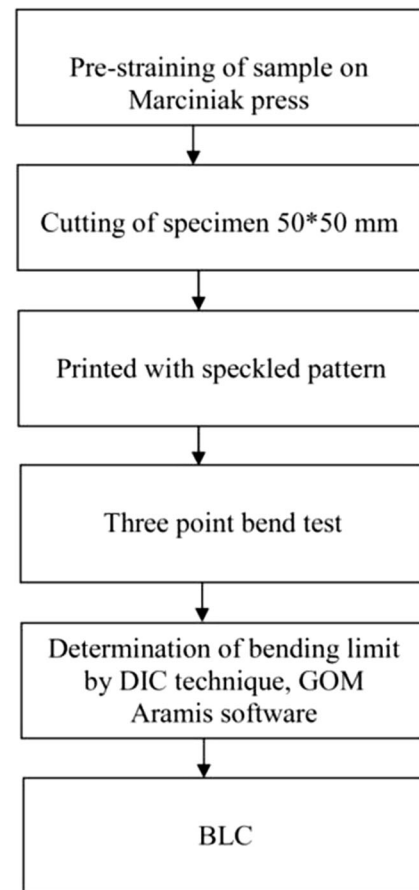


**Fig. 16** Flow chart of experimental approach

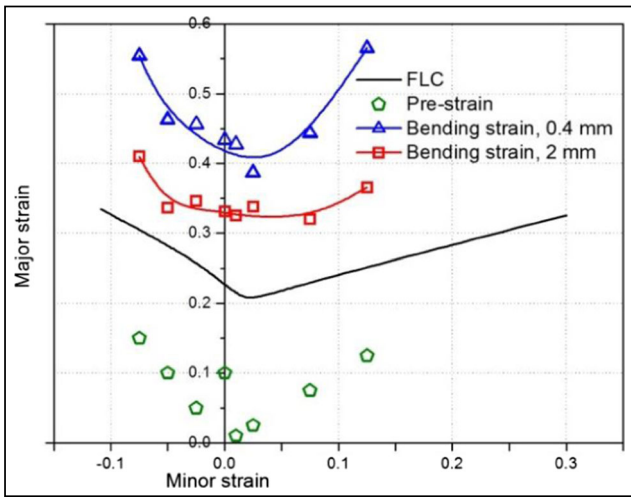


Fig. 17 Combined BLC and FLC for Al6014

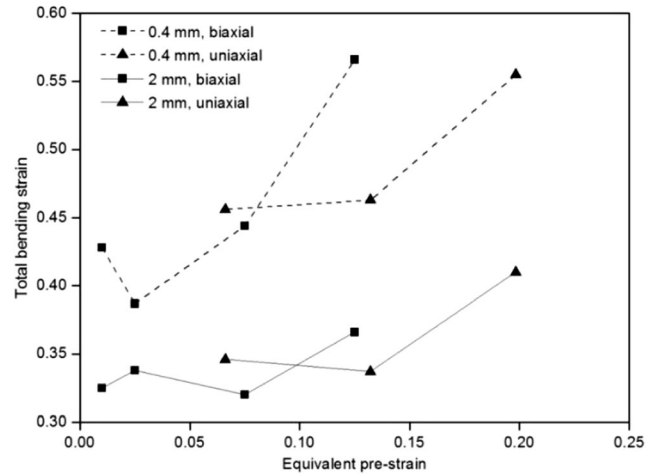


Fig. 19 Plot between total bending strain and equivalent pre-strain

The regression equation for the total bending strain for Al6014 is represented as Eq. 5.

$$\begin{aligned} \phi_{BL} = & 0.400448 + 1.19481 \times \phi_{eq} - 0.00653186 \\ & \times \alpha - 0.050684 \times r + 0.28722 \times \phi_{eq} \\ & \times \alpha - 0.311286 \times \phi_{eq} \times r + 0.01465 \times \alpha \\ & \times r - 0.316592 \times \phi_{eq} \times \alpha \times r \end{aligned} \quad (5)$$

The normal probability plot for the regression model is shown in Fig. 26 and the ANOVA table for the regression model is shown in Table 6.

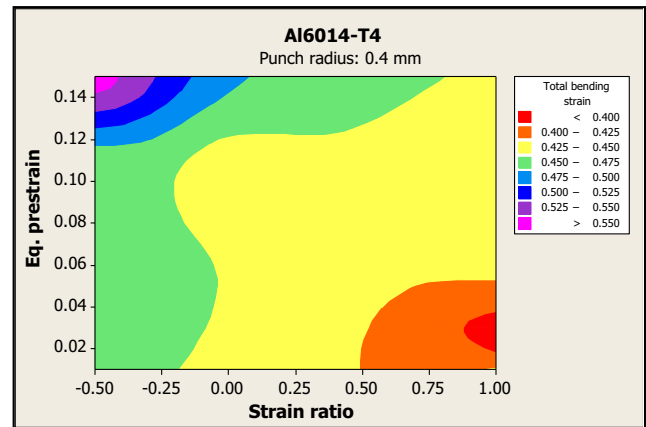


Fig. 20 Variation of total bending strain with equivalent pre-strain and strain ratio, 0.4 mm punch radius

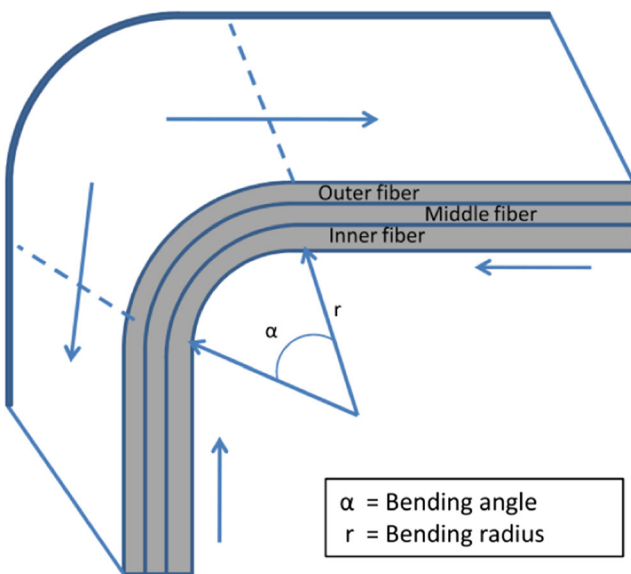


Fig. 18 Bend specimen showing top, middle and bottom fiber

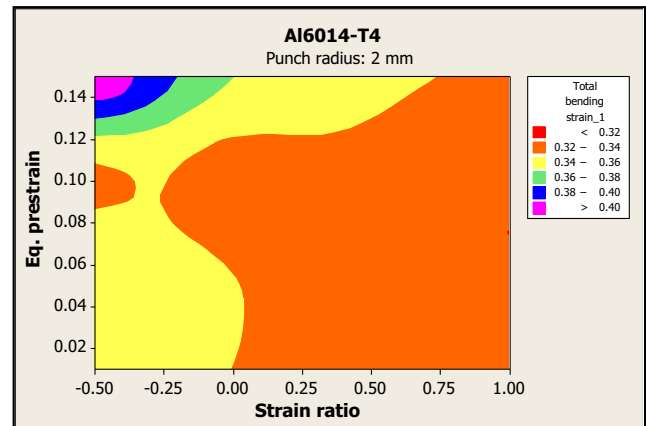


Fig. 21 Variation of total bending strain with equivalent pre-strain and strain ratio, 2 mm punch radius



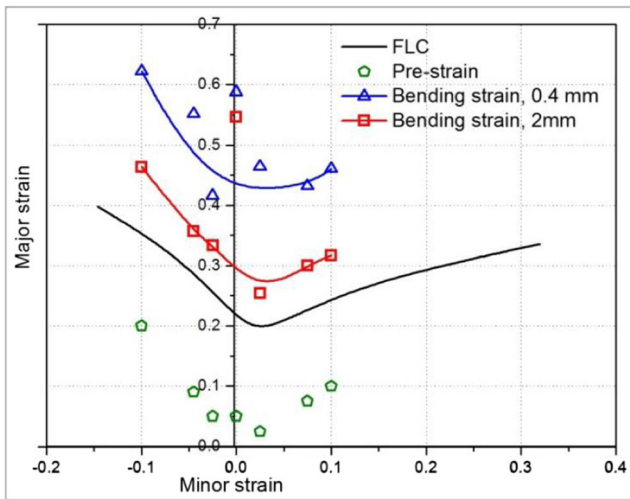


Fig. 22 Combined BLC and FLC for DP600

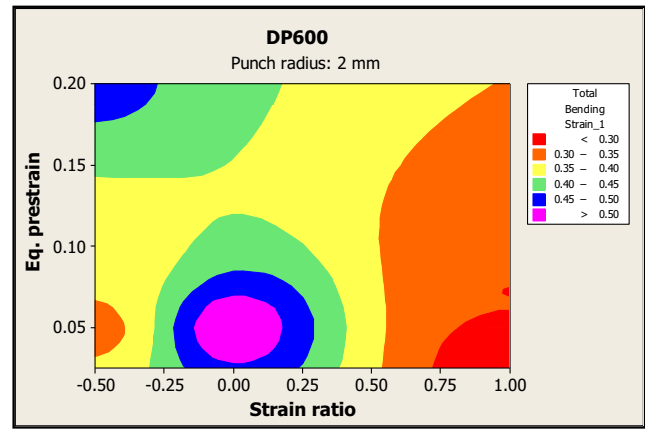


Fig. 25 Variation of total bending strain with respect to equivalent pre-strain and strain ratio, 2 mm punch radius

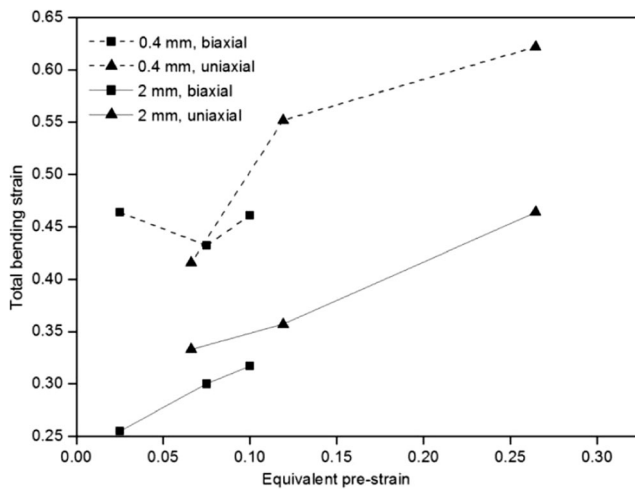


Fig. 23 Plot between total bending strain and equivalent pre-stain for DP600

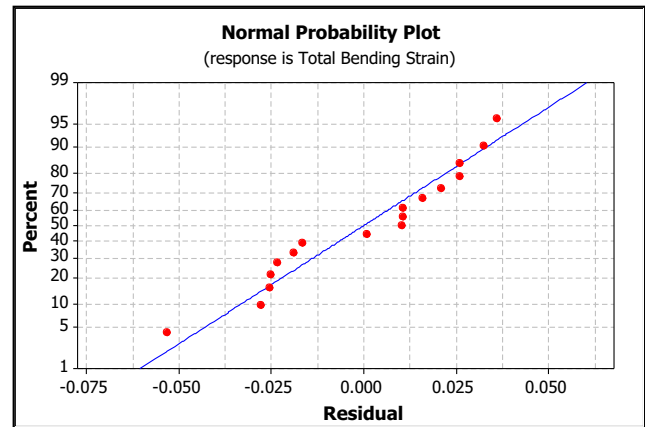


Fig. 26 Normal probability plot for regression model of Al-6014

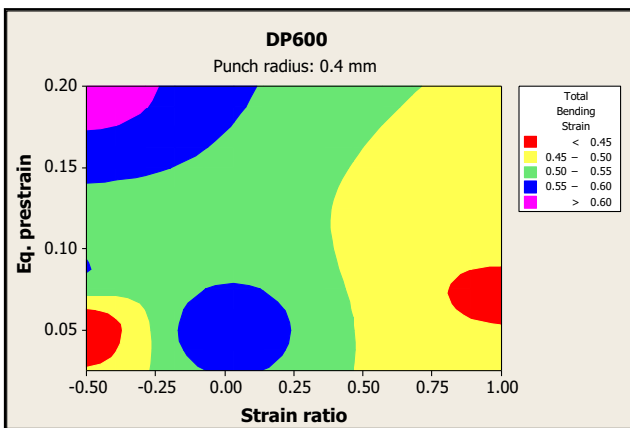


Fig. 24 Variation of total bending strain with respect to equivalent pre-strain and strain ratio, 0.4 mm punch radius

Table 6 ANOVA for regression fit for Al6014

Source	DF	Seq SS	Adj SS	Adj MS	F	P
Regression	7	0.0800086	0.0800086	0.0114298	9.52322	0.001550
$\phi_{eq}$	1	0.0160136	0.0086719	0.0086719	7.22536	0.024878
$\alpha$	1	0.0002175	0.0000200	0.0000200	0.01670	0.900028
$r$	1	0.0592986	0.0031836	0.0031836	2.65255	0.137825
$\phi_{eq} \times \alpha$	1	0.0001013	0.0003595	0.0003595	0.29949	0.597507
$\phi_{eq} \times r$	1	0.0027484	0.0013749	0.0013749	1.14554	0.312348
$\alpha \times r$	1	0.0006352	0.0002194	0.0002194	0.18277	0.679050
$\phi_{eq} \times \alpha \times r$	1	0.0009941	0.0009941	0.0009941	0.82825	0.386504
Error	9	0.0108018	0.0108018	0.0012002		
Lack-of-fit	8	0.0108018	0.0108018	0.0013502		
Pure error	1	0.0000000	0.0000000	0.0000000		
Total	16	0.0908105				

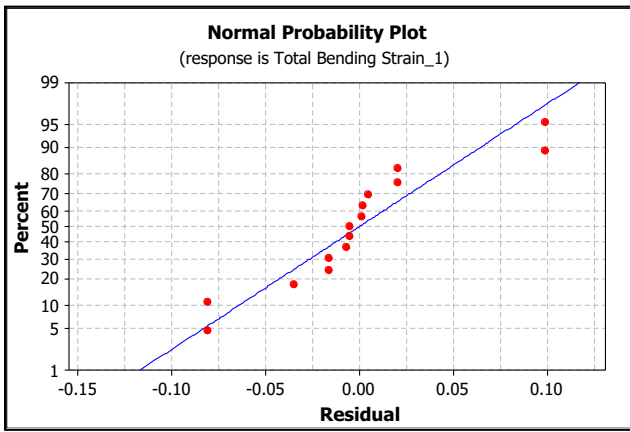


Fig. 27 Normal probability plot for the regression model of DP600

The regression equation for the total bending strain for DP600 is given by Eq. 6.

$$\begin{aligned} \phi_{BL} = & 0.507074 + 0.483857 \times \phi_{eq} + 0.0224271 \\ & \times \alpha - 0.106284 \times r - 0.760943 \times \phi_{eq} \times \alpha \\ & + 0.015073 \times \phi_{eq} \times r \end{aligned} \tag{6}$$

Normal probability plot for the regression model in case of DP600 is shown in Fig. 27 and the ANOVA table for the regression model is shown in Table 7.

The minor strain can be obtained by using Eqs. 1 & 3. The point of failure in the BLC can be determined by coordinates in Eq. 7.

$$P = \begin{bmatrix} \phi_{BL} \\ \phi_2 \end{bmatrix} \tag{7}$$

Table 7 ANOVA for regression fit for DP600

Source	DF	Seq SS	Adj SS	Adj MS	F	P
Regression	5	0.085897	0.0858974	0.0171795	4.37440	0.026848
$\phi_{eq}$	1	0.022418	0.0037936	0.0037936	0.96595	0.351372
$\alpha$	1	0.000576	0.0006897	0.0006897	0.17562	0.684987
$r$	1	0.057896	0.0147903	0.0147903	3.76603	0.084225
$\phi_{eq} \times \alpha$	1	0.005002	0.0047179	0.0047179	1.20133	0.301518
$\phi_{eq} \times r$	1	0.000005	0.0000049	0.0000049	0.00124	0.972718
Error	9	0.035345	0.0353455	0.0039273		
Lack-of-fit	4	0.035345	0.0353455	0.0088364		
Pure error	5	0.000000	0.000000	0.000000		
Total	14	0.121243				

### Conclusion

In the present work, bending limit curve for AA6014-T4 and DP600 were evaluated. Forming limits and bending limits for both the materials were determined by DIC technique using GOM Aramis software. In case of both Al6014-T4 & DP600, BLCs were found to be at a higher level than conventional FLCs. Furthermore, effect of punch radius as well as level and nature of pre-strain was studied on bending strain. Lower bending strain was observed with higher punch radius. Because of the micro structural changes during bending as well as mechanical properties, nature of bending strain varied with the level of pre-strain. The regression model can be used to predict bending limits at arbitrary load ratios. The BLCs can be implemented as a post processing criterion in the bending/hemming process simulations. The future scope of the work lies in validating such applications in finite element based forming simulations.

FLC, Forming Limit Curve; BLC, Bending Limit Curve;  $\phi_1$ , Major strain;  $\phi_2$ , Minor strain;  $\phi_{BL}$ , Total bending strain or bending limit strain;  $\phi_{eq}$ , Equivalent strain; ANOVA, Analysis of Variance;  $\phi_b$ , Bending strain;  $\phi_{1p}$ , Major pre-strain;  $\alpha$ , Strain ratio; HSLA, High strength low alloy

**Acknowledgments** The authors are thankful to Prof. Mathias Liewald, Dr.-Ing Stefan Wagner, Dipl.-Ing Klaus Drotleff and Staff of Institut für Umformtechnik for providing useful resources and facilities for carrying out the experiments. Their support during the research work is highly acknowledged.

### References

- Keeler SP (1965) Determination of forming limits in automobile stamping. Sheet Met Ind 42:683
- Keeler SP, Backofen WA (1963) Plastic instability and fracture in sheets stretched over rigid punches. In: Trans. ASM
- Goodwin GM (1968) Application of strain analysis to sheet metal forming problems in press shop. SAE Pap. No. 680093
- Denninger R, Liewald M, Held C, Sindel M (2011) Investigations on bendability of lightweight materials for various load paths. Mater Form ESAFORM. doi:10.1063/1.3589745
- Schleich R, Sindel M, Liewald M (2009) Investigation on the effect of curvature on forming limit prediction for aluminium sheet alloys. Int J Mater Form 2:69–74. doi:10.1007/s12289-009-0394-z
- Wagner S, Liewald M (2013) Improved failure description in forming of automotive sheet metal parts. Acad J Manuf Eng 11: 1–8
- Sarkar J, Kutty TRG, Conlon KT et al (2001) Tensile and bending properties of AA5754 aluminum alloys. Mater Sci Eng A 316:52–59. doi:10.1016/S0921-5093(01)01226-6
- Sarkar J, Kutty TRG, Wilkinson DS et al (2004) Tensile properties and bendability of T4 treated AA6111 aluminum alloys. Mater Sci Eng A 369:258–266. doi:10.1016/j.msea.2003.11.022
- Liewald M, Sindel M, Schleich R, Held C (2008) Beitrag zur Verbesserung der simulativen Absicherung von biegedominierten Umformprozessen im Automobilbau. GRIPS Media Verlag. doi: 10.1007/BF02833650

10. Lin G, Hu SJ, Cai W (2009) Evaluation of formability in bending/hemming of aluminum alloys using plane-strain tensile tests. *J Manuf Sci Eng* 131:051009. doi:[10.1115/1.3123316](https://doi.org/10.1115/1.3123316)
11. Kitting D, Ofenheimer A, Pauli H, Till ET (2010) A phenomenological concept to predict formability in stretch-bending forming operations. *Int J Mater Form* 3:1163–1166. doi:[10.1007/s12289-010-0979-6](https://doi.org/10.1007/s12289-010-0979-6)
12. Le Maoût N, Thuillier S, Manach PY (2010) Drawing, flanging and hemming of metallic thin sheets: a multi-step process. *Mater Des* 31:2725–2736. doi:[10.1016/j.matdes.2010.01.030](https://doi.org/10.1016/j.matdes.2010.01.030)
13. Hu Y, Han Y, Yao Z, Hu J (2010) Three-dimensional numerical simulation and experimental study of sheet metal bending by laser peen forming. *J Manuf Sci Eng* 132:061001. doi:[10.1115/1.4002585](https://doi.org/10.1115/1.4002585)
14. Thuillier S, Le Maoût N, Manach PY (2011) Influence of ductile damage on the bending behaviour of aluminium alloy thin sheets. *Mater Des* 32:2049–2057. doi:[10.1016/j.matdes.2010.11.050](https://doi.org/10.1016/j.matdes.2010.11.050)
15. Pedersen KO, Børvik T, Hopperstad OS (2011) Fracture mechanisms of aluminium alloy AA7075-T651 under various loading conditions. *Mater Des* 32:97–107. doi:[10.1016/j.matdes.2010.06.029](https://doi.org/10.1016/j.matdes.2010.06.029)
16. Zadpoor AA, Campoli G, Sinke J, Benedictus R (2011) Fracture in bending - the straining limits of monolithic sheets and machined tailor-made blanks. *Mater Des* 32:1229–1241. doi:[10.1016/j.matdes.2010.10.005](https://doi.org/10.1016/j.matdes.2010.10.005)
17. Davidkov A, Jain MK, Petrov RH et al (2012) Strain localization and damage development during bending of Al–Mg alloy sheets. *Mater Sci Eng A* 550:395–407. doi:[10.1016/j.msea.2012.04.093](https://doi.org/10.1016/j.msea.2012.04.093)
18. Denninger R, Liewald M, Sindel M (2012) Failure prediction in sheet metal forming depending in pre-straining and bending superposition. In: *Mater. Form. ESAFORM 2012*. Trans Tech Publications, Switzerland, pp 101–106
19. He J, Cedric Xia Z, Li S, Zeng D (2013) M–K analysis of forming limit diagram under stretch-bending. *J Manuf Sci Eng* 135:041017. doi:[10.1115/1.4024536](https://doi.org/10.1115/1.4024536)
20. Shi Y, Jin H, Wu PD et al (2014) Failure analysis of fusion clad alloy system AA3003/AA6xxx sheet under bending. *Mater Sci Eng A* 610:263–272. doi:[10.1016/j.msea.2014.05.047](https://doi.org/10.1016/j.msea.2014.05.047)
21. Liewald M, Drotleff K (2014) Concept of the bending limit curve. In: *FLC 2014 Work*. Novemb. 6 7, 2014, Zurich, Switz. pp 17–22
22. (2008) *Metallic materials-sheets and strips-determination of forming curves*. Int. Stand. 12004–2
23. (2009) *Standard test methods for tension testing of metallic materials*, ASTM\_E8 standard
24. Hatch JE (1984) *Aluminum: properties and physical metallurgy*
25. (2010) *VDA 238–100, Plate bending test for metallic materials*. 1–13
26. Mises RV (1913) *Mechanik der festen Körper im plastisch-deformablen Zustand*. Nachrichten von der Gesellschaft der Wissenschaften zu Göttingen. Math Klasse 582–592